Upwind Finite Difference Schemes for the Computation of Traveltime in Transversely Isotropic Media with Vertical Symmetry Axis

*Jian L. Qian *and William W. Symes †*

ABSTRACT

We apply our general mathematical formulations of finite difference schemes for the computation of traveltime and amplitude in inhomogeneous anisotropic media to the transversely isotropic media with vertical symmetry axis (VTI).

The Hamilton-Jacobi equation for the downgoing qP wave is given in terms of Thomsen parameters and a second order Essentially Nonoscillatory(ENO) Hamilton-Jacobi solver is applied to get the viscosity solution (the first-arrival traveltime field) on a regular grid.Numerical experiments (2D and 3D) and tests on the isotropic and an anisotropic Marmousi model show that our approach is efficient and accurate.

Introduction

Anisotropic traveltime computations play an important role in many methods of seismic data processing, such as anisotropic DMO and anisotropic migration (Tsvankin, 1995; Alkhalifah, 1996; Anderson, 1996). These traveltimes are often computed by ray tracing (Cerveny, 1972);and because depth and surface points are usually distributed on a regular grid,the traveltime along the rays are then interpolated on to the grid. For complicated velocity model,rays may cross each other or not penetrate shadow zones, the interpolation are thus cumbersome and computationally expensive.

Although many methods have been introduced to compute the traveltime for isotropic media directly on regular grid (Reshef and Kosloff, 1986; Vidale, 1988; van Trier and Symes, 1991; Schneider, 1995; Kim and Cook, 1998), there is still no

*The Rice Inversion Project,Department of Computational and Applied Mathematics,Rice University,Houston TX 77251-1892 USA,email jlqian@caam.rice.edu

†The Rice Inversion Project,Department of Computational and Applied Mathematics,Rice University,Houston TX 77251-1892 USA,email symes@caam.rice.edu

promising algorithm for the traveltime in anisotropic media on regular grid.Dellinger and Symes (Dellinger, 1991; Dellinger and Symes, 1997) have investigated the possibility of using upwind finite difference schemes to compute the first-arrival traveltime in anisotropic media, but they did not give an explicit and specific approach to compute the traveltime and amplitude.

From the viewpoint of mathematical physics,the first arrival traveltime in the isotropic media is the unique viscosity solution of the Hamilton-Jacobi (HJ)equation which is derived from the corresponding eikonal equation (Lions, 1982; Crandall and Lions, 1983; Crandall et al., 1984),so that we have the uniqueness of first-arrival traveltime in the isotropic media. van Trier and Symes (van Trier and Symes, 1991),Symes et al.(1994),(El-Mageed, 1996),Kim et al. (El-Mageed et al., 1997) have computed this viscosity solution(the first-arrival traveltime) successfully by using ENO(essentially non-oscillatory) upwind finite difference schemes which were introduced by Osher and Sethian (Osher and Sethian, 1988) and Osher and Shu (Osher and Shu, 1991). Motivated by their success in isotropic media,we obtained mathematical formulations for the computation of first-arrival traveltime field in general inhomogeneous anisotropic media by upwind finite difference schemes (Qian and Symes, 1998).

The goal of this paper is to apply our general mathematical formulations to the special case,i.e. transversely isotropic media with vertical symmetry axis (VTI). The Hamilton-Jacobi equation in terms of Thomsen's parameter is given for the downgoing qP wave propagation and a second order ENO-HJ solver is used to get the corresponding viscosity solution. The Courant-Friedrichs-Levy(CFL) condition necessary for stability of explicit finite difference schemes shows that it is important to enforce a limited aperture (maximum phase angle condition) so as to reduce the computational cost. Two- and three-dimensional numerical experiments and tests on the isotropic and an anisotropic Marmousi model demonstrate that our proposed approach is efficient and accurate.

Hamilton-Jacobi equation in 3D VTI

The elastic modulus matrix for transversely isotropic media with vertical symmetry axis (VTI) has five independent components among twelve nonzero components (Musgrave, 1970; Thomsen, 1986),the characteristic polynomial equation corresponding to the eikonal equation in VTI equals

$$\begin{vmatrix} a_{11}p_1^2 + a_{66}p_2^2 + a_{44}p_3^2 - 1 & (a_{12}+a_{66})p_1p_2 & (a_{13}+a_{44})p_1p_3 \\ (a_{12}+a_{66})p_1p_2 & a_{66}p_1^2 + a_{11}p_2^2 + a_{44}p_3^2 - 1 & (a_{13}+a_{44})p_2p_3 \\ (a_{13}+a_{44})p_1p_3 & (a_{13}+a_{44})p_2p_3 & a_{44}p_1^2 + a_{44}p_2^2 + a_{33}p_3^2 - 1 \end{vmatrix} = 0,$$

where a_{11},a_{33},a_{44},a_{66} and a_{13} are elastic parameters normalized by density,and the slowness vector p is $p_1 = \frac{\partial \tau}{\partial x}$,$p_2 = \frac{\partial \tau}{\partial y}$ and $p_3 = \frac{\partial \tau}{\partial z}$.

If we are interested in first-arrival traveltime (TT),it corresponds to downgoing qP wave,i.e. $p_3 > 0$,hence we have a Hamilton-Jacobi equation for VTI media with respect to downgoing qP wave by our general formulation (Qian and Symes, 1998):

$$\begin{aligned} p_3 &= H(p_1, p_2) \\ &= \sqrt{\frac{2c}{-b + \sqrt{b^2 - 4ac}}} \end{aligned} \tag{1}$$

i.e.,

$$\frac{\partial \tau}{\partial z} = H\left(\frac{\partial \tau}{\partial x}, \frac{\partial \tau}{\partial y}\right). \tag{2}$$

where

$$\begin{aligned} a &\equiv a_{33}a_{44}, \\ b &\equiv (a_{11}a_{33} + a_{44}^2 - (a_{13} + a_{44})^2)(p_1^2 + p_2^2) - a_{33} - a_{44}, \\ c &\equiv (a_{11}(p_1^2 + p_2^2) - 1)(a_{44}(p_1^2 + p_2^2) - 1). \end{aligned} \tag{3}$$

We note that the above coefficient $b = b(p_1, p_2)$ is nonpositive,and its coefficient with respect to $(p_1^2 + p_2^2)$ is nonnegative by Postma and Berryman's inequality (Berryman, 1979). By $b = b(p_1, p_2)$ nonpositive,the HJ equation formulated above can avoid the numerical cancellation in practice.

To justify the upwind direction, we need the partial derivatives which are given by

$$\frac{\partial H}{\partial p_1} = -\frac{r_1}{r_3}, \tag{4}$$

$$\frac{\partial H}{\partial p_2} = -\frac{r_2}{r_3}. \tag{5}$$

where

$$\begin{aligned} r_1(p_1, p_2, p_3) &= p_1(2a_{11}a_{44}(p_1^2 + p_2^2) + Ap_3^2 - a_{11} - a_{44}), \\ r_2(p_1, p_2, p_3) &= p_2(2a_{11}a_{44}(p_1^2 + p_2^2) + Ap_3^2 - a_{11} - a_{44}), \\ r_3(p_1, p_2, p_3) &= p_3(2a_{33}a_{44}p_3^2 + A(p_1^2 + p_2^2) - a_{33} - a_{44}), \end{aligned} \tag{6}$$

$$A = a_{11}a_{33} + a_{44}^2 - (a_{13} + a_{44})^2,$$

The above formulae follow from general forms in (Qian and Symes, 1998).

The phase velocity of qP wave is given by Thomsen (Thomsen, 1986):

$$v_{qP}^2(\theta) = \frac{1}{2}\left(Y_0 + Y_1 + \sqrt{(Y_0 - Y_1)^2 + 4Y_2}\right), \tag{7}$$

where

$$
\begin{aligned}
Y_0(\theta) &\equiv a_{11}\sin^2\theta + a_{44}\cos^2\theta,\\
Y_1(\theta) &\equiv a_{44}\sin^2\theta + a_{33}\cos^2\theta,\\
Y_2(\theta) &\equiv (a_{13}+a_{44})^2\sin^2\theta\cos^2\theta.
\end{aligned}
$$

Thomsen parameters for VTI media

The above formulation needs to know the five elastic parameters in VTI, which is difficult to obtain in the reflection seismology,Thomsen(1986) recasted the above formulation by using only two elastic moduli(i.e.,vertical qP and vertical qS wave velocities) and introducing three measures of anisotropy to replace the other three parameters.

The vertical sound speeds for qP and qS waves are $\sqrt{a_{33}}$ and $\sqrt{a_{44}}$, and the horizontal sound speeds for qP and qS waves are $\sqrt{a_{11}}$ and $\sqrt{a_{66}}$. Thomsen(1986) defined five parameters as follows:

$$
\begin{aligned}
\alpha_0 &\equiv \sqrt{a_{33}}\\
\beta_0 &\equiv \sqrt{a_{44}}\\
\epsilon &\equiv \frac{a_{11}-a_{33}}{2a_{33}}\\
\gamma &\equiv \frac{a_{66}-a_{44}}{2a_{44}}\\
\delta &\equiv \frac{(a_{13}+a_{44})^2-(a_{33}-a_{44})^2}{2a_{33}(a_{33}-a_{44})}
\end{aligned}
\tag{8}
$$

where ϵ is the fractional difference between the vertical and horizontal P-velocities,γ the fractional difference between the vertical and horizontal S-velocities, and δ controls the near-vertical anisotropic qP-wave propagation.

Hence the elastic parameters can be expressed as the functions of Thomsen parameters:

$$
\begin{aligned}
a_{33} &\equiv \alpha_0^2\\
a_{44} &\equiv \beta_0^2\\
a_{11} &\equiv \alpha_0^2(1+2\epsilon)\\
a_{66} &\equiv \beta_0^2(1+2\gamma)\\
a_{13} &\equiv ((\alpha_0^2-\beta_0^2)^2+2\alpha_0^2(\alpha_0^2-\beta_0^2)\delta)^{\frac{1}{2}}-\beta_0^2
\end{aligned}
\tag{9}
$$

By using Thomsen parameters,we have new expressions for coefficients a, b, c in the Hamilton-Jacobi equation for qP wave in VTI:

$$
\begin{aligned}
a &\equiv \alpha_0^2\beta_0^2\\
b &\equiv 2\alpha_0^2\beta_0^2(1+\delta+(\epsilon-\delta)\frac{\alpha_0^2}{\beta_0^2})(p_1^2+p_2^2)-\alpha_0^2-\beta_0^2\\
c &\equiv ((1+2\epsilon)\alpha_0^2(p_1^2+p_2^2)-1)(\beta_0^2(p_1^2+p_2^2)-1).
\end{aligned}
\tag{10}
$$

ENO schemes for VTI media

Given mesh sizes Δx,Δy,Δz, denote grid points as

$$(x_m, y_k, z_n) = (x_{\min} + (m-1)\Delta x, y_{\min} + (k-1)\Delta y, z_{\min} + (n-1)\Delta z), \quad (11)$$

the numerical approximation to the viscosity solution $\tau(x_m, y_k, z_n)$ of Hamilton-Jacobi equation (1) at the grid point (x_m, y_k, z_n) is denoted as

$$\tau^n_{m,k} = \tau(x_m, y_k, z_n),$$

define the backward (-) and forward (+) first order difference quotient approximations to the left and right derivatives of $\tau(x, y, z)$ at the location (x_m, y_k, z_n) with respect to x and y:

$$\begin{aligned} D^{\pm}_x \tau^n_{m,k} &= \pm\frac{\tau^n_{m\pm 1,k} - \tau^n_{m,k}}{\Delta x}, \\ D^{\pm}_y \tau^n_{m,k} &= \pm\frac{\tau^n_{m,k\pm 1} - \tau^n_{m,k}}{\Delta y}. \end{aligned} \quad (12)$$

We adapt Godunov type monotone numerical Hamiltonian to approximate the Hamiltonian H in (1),the first-order upwind scheme follows:

$$\tau^{n+1}_{m,k} = \tau^n_{m,k} + \Delta z_{CFL} H[\tau]^n_{m,k} \quad (13)$$

where Δz satisfies the CFL condition and $H[\tau]^n_{m,k}$ is computed by Godunov's scheme,

$$H[\tau]^n_{m,k} = H\left((\hat{p}_1)^n_{m,k}, (\hat{p}_2)^n_{m,k}\right). \quad (14)$$

We remark that if the Hamiltonian is convex,then

$$\begin{aligned} (\hat{p}_1)^n_{m,k} &= maxmod(\max(D^-_x \tau^n_{m,k}, 0), \min(D^+_x \tau^n_{m,k}, 0)), \\ (\hat{p}_2)^n_{m,k} &= maxmod(\max(D^-_y \tau^n_{m,k}, 0), \min(D^+_y \tau^n_{m,k}, 0)), \end{aligned} \quad (15)$$

which is similar to the isotropic case.In general,we must use the derivatives $\frac{\partial H}{\partial p_1}$ and $\frac{\partial H}{\partial p_2}$ to justify the upwind direction.

To get higher order schemes,the above numerical Hamiltonian will be used as buliding blocks,the first order approximation to the derivative will be replaced by higher order ENO approximation. And along the z-direction the higher order TVD Runge-Kutta schemes (Shu and Osher, 1988) will be used to match the higher order ENO schemes for the other variables.

To derive a second-order scheme,use the following second order ENO finite difference to approximate the first order derivative $\frac{\partial \tau}{\partial x}$ (Osher and Sethian, 1988)

$$\begin{aligned} D_x^{+,2}\tau &= D_x^+\tau - \frac{1}{2}\Delta x m(D_x^+D_x^+\tau, D_x^-D_x^+\tau), \\ D_x^{-,2}\tau &= D_x^-\tau + \frac{1}{2}\Delta x m(D_x^-D_x^-\tau, D_x^-D_x^+\tau) \end{aligned} \tag{16}$$

where

$$m(x,y) = \begin{cases} x & \text{if } |x| <= |y| \text{ and } xy > 0, \\ y & \text{if } |y| < |x| \text{ and } xy > 0, \\ 0 & \text{if } xy <= 0. \end{cases} \tag{17}$$

Introduce the analogues for $\frac{\partial \tau}{\partial y}$.

Then ENO-HJ second-order scheme follows :

$$\begin{aligned} \tau_{m,k}^{n+\frac{1}{2}} &= \tau_{m,k}^n + \Delta z_{CFL} H[\tau]_{m,k}^n, \\ \tau_{m,k}^{n+1} &= \frac{1}{2}(\tau_{m,k}^n + \tau_{m,k}^{n+\frac{1}{2}} + \Delta z_{CFL} H[\tau]_{m,k}^{n+\frac{1}{2}}) \end{aligned} \tag{18}$$

where $H[\tau]_{m,k}^n$ is computed by our Godunov scheme with the second order ENO approximation to $p_1 = \frac{\partial \tau}{\partial x}$ and $p_2 = \frac{\partial \tau}{\partial y}$, Δz_{CFL} is the CFL step,

$$H[\tau]_{m,k}^n = H\left((\hat{p}_1)_{m,k}^n, (\hat{p}_2)_{m,k}^n\right). \tag{19}$$

Now we consider the stability condition. For given consistent finite difference schemes solving evolution partial differential equations, the $Courant-Friedrichs-Levy$ (CFL) stability condition states that the numerical domain of dependence of the discretized PDE contains the physical domain of dependence of PDE (LeVeque, 1990).

Linearize the eikonal equation (1) for qP wave with respect to p_1, p_2 and p_3

$$ap_3^4 + b(p_1,p_2)p_3^2 + c(p_1,p_2) = 0, \tag{20}$$

we have

$$r_3(p_1,p_2,p_3)\delta p_3 + r_2(p_1,p_2,p_3)\delta p_2 + r_1(p_1,p_2,p_3)\delta p_1 = 0 \tag{21}$$

where r_1,r_2 and r_3 are defined in (6).So

$$\begin{aligned} \frac{\partial H}{\partial p_1} &= \frac{\partial p_3}{\partial p_1} \\ &= -\frac{r_1}{r_3}, \end{aligned} \tag{22}$$

$$
\begin{aligned}
\frac{\partial H}{\partial p_2} &= \frac{\partial p_3}{\partial p_2} \\
&= -\frac{r_2}{r_3}.
\end{aligned} \tag{23}
$$

Thus the CFL condition necessary for stability is

$$
\Delta z_{CFL} \left(\max_{p_1,p_2} \sqrt{\left(\frac{\partial H}{\partial p_1}\right)^2 + \left(\frac{\partial H}{\partial p_2}\right)^2} \right) \leq \frac{\Delta x \Delta y}{\sqrt{\Delta x^2 + \Delta y^2}}. \tag{24}
$$

or

$$
\Delta z_{CFL} \max_{p_1,p_2} \left| \frac{\sqrt{r_1^2 + r_2^2}}{r_3} \right| \leq \frac{\Delta x \Delta y}{\sqrt{\Delta x^2 + \Delta y^2}}. \tag{25}
$$

where the maximum is taken over the relevant range of p_1 and p_2.

We should avoid choosing very small step size in the $z-$direction because a small step size increases the computational cost, and it may cause a severe numerical diffusion/dispersion since it diminishes the physical domain of dependence(Strikwerda, 1989).

By the CFL condition, one can see that r_3 controlling the CFL step is dominated by p_3,so one should avoid p_3 going to zero which is achieved by enforcing the maximum phase angle condition.

The slowness vector for qP wave in VTI is

$$
\begin{aligned}
p_1 &= \frac{\sin\theta\cos\phi}{v_{qp}(\theta)}, \\
p_2 &= \frac{\sin\theta\sin\phi}{v_{qp}(\theta)}, \\
p_3 &= \frac{\cos\theta}{v_{qp}(\theta)},
\end{aligned} \tag{26}
$$

where θ is the angle between the normal vector to the qP wave front and the z axis,ϕ is in between 0 and 2π. In VTI case,v_{qP} depends only on θ.

Given θ_{max},let $|\theta| \leq \theta_{\max}$,then

$$
p_3 \geq \frac{\cos(\theta_{\max})}{v_{qp}(\theta_{\max})}, \tag{27}
$$

we have a modified Hamilton Jacobi equation for qP wave

$$
p_3 = \sqrt{bmax\left(\frac{2c}{-b+\sqrt{b^2-4ac}}, \frac{\cos^2(\theta_{\max})}{v_{qp}^2(\theta_{\max})}\right)} \tag{28}
$$

where $bmax$ is a piecewise quadratic function,

$$\begin{aligned} bmax(x,y) &= y \text{ if } |x| \leq 0 \\ &= y + \frac{x^2}{4y} \text{ if } 0 \leq x \leq 2y \\ &= x \text{ if } x \geq 2y. \end{aligned}$$

In effect we have modified the wavefront: the part with near vertical normals is unaffected, but the steeper part is replaced by a plane wave, so that we have a limited aperture with $2\theta_{\max}$.

Numerical Experiments: 2D VTI media

We have performed several numerical experiments to verify that our approach is feasible and promising.

In all examples,traveltimes for qP wave propagation in VTI media are computed. All models occupy the rectangle $\{-0.5km \leq x \leq 0.5km, 0 \leq z \leq 1km\}$,the source is located at the surface in the middle of the model.Maximum phase angle is taken as $\theta_{\max} = 4\pi/9$,$\Delta x = \Delta z = 0.01$. Ray-tracing method is used to calibrate our code (Cerveny and Psencik, 1972).

The elastic parameters in the following examples are designed to satisfy stress-strain coefficient inequalities in (Berryman, 1979) according to their Thomsen's parameters in homogeneous situation.

Example 1. The four elastic parameters are:

$$\begin{aligned} a_{11} &= 15.4136 + 2z \\ a_{33} &= 11.0889 + z \\ a_{44} &= 3.1329 + 0.5z \\ a_{13} &= 1.8148 + 0.5z \end{aligned}$$

which are perturbations to Thomsen's parameters for homogeneous Green River Shale:

$$\begin{aligned} \alpha_0 &= 3.33km/s, \\ \beta_0 &= 1.77km/s, \\ \epsilon &= 0.195, \\ \delta &= -0.220. \end{aligned}$$

See Figure 1 to Figure 4.

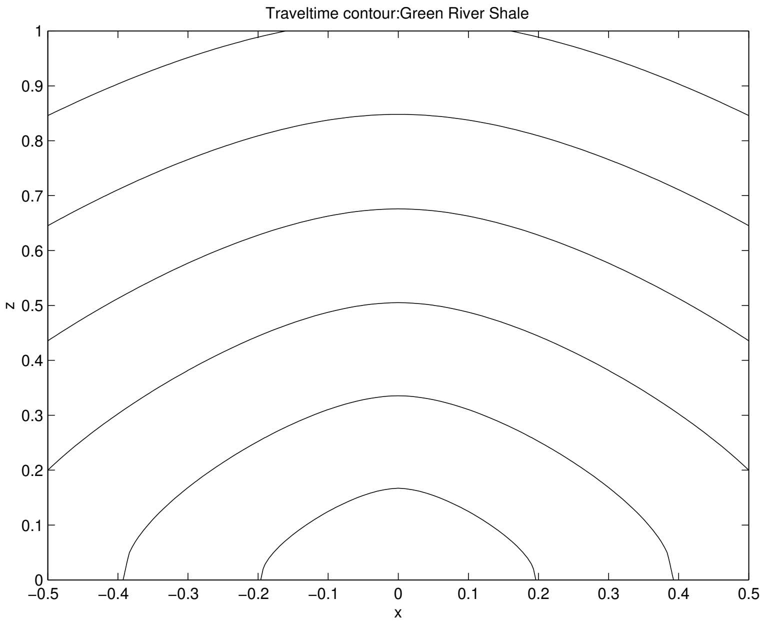

FIG. 1. Wavefront:Example 1

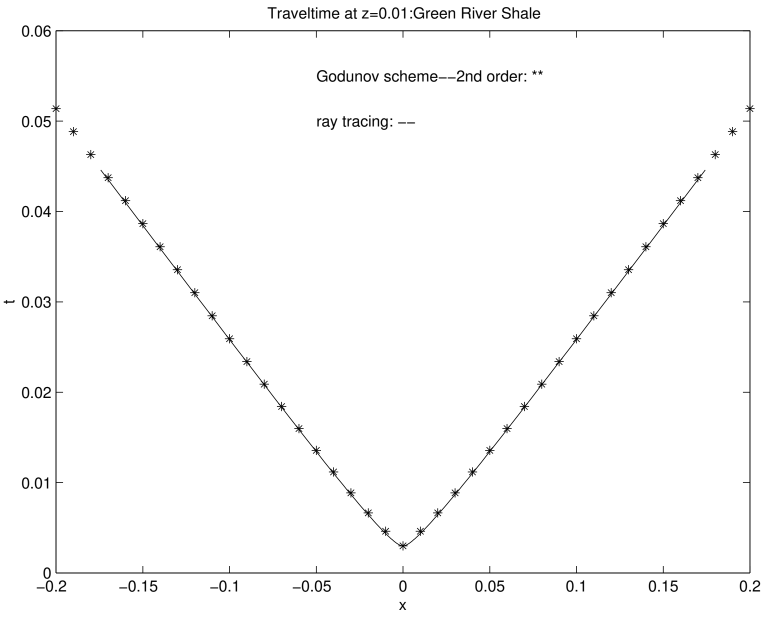

FIG. 2. ENO TT and Raytracing TT near surface:Example 1

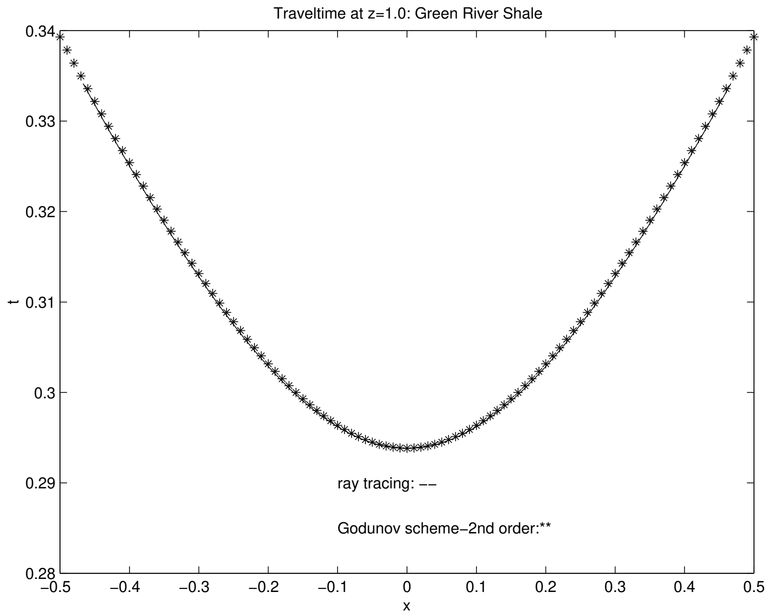

FIG. 3. ENO TT and Raytracing TT at bottom:Example 1

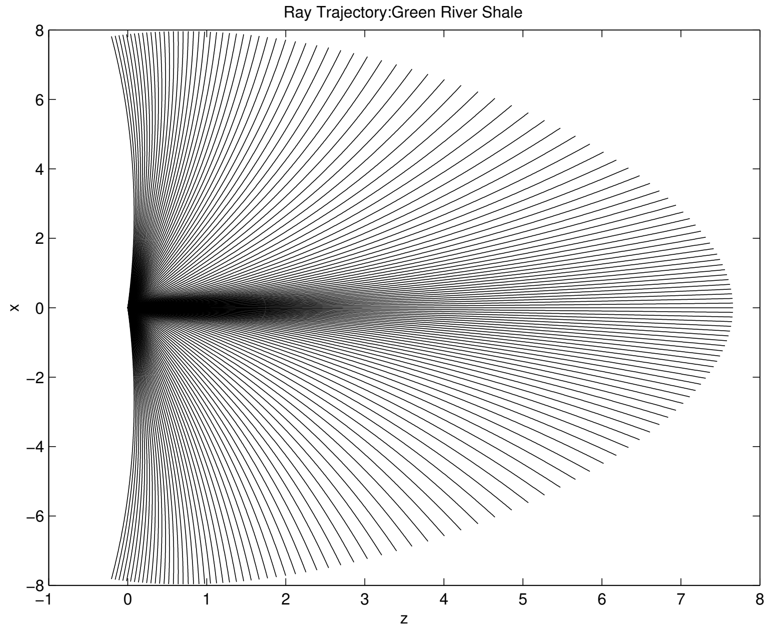

FIG. 4. Raytracing:Example 1

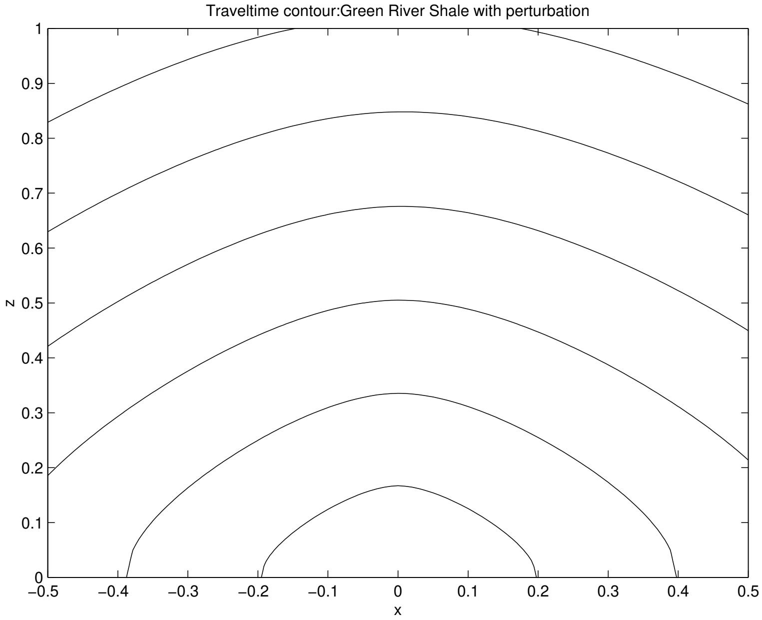

FIG. 5. Wavefront: Example 2

Table 1. Convergence Rates of Relative Errors in computed TT

h	E(τ,h)	α(τ,h)
0.02	0.00215	
0.01	0.00100	1.098
0.005	4.313e-04	1.222
0.0025	1.438e-04	1.585

Example 2. The four elastic parameters are:

$$\begin{aligned} a_{11} &= 15.4136 + 2x + 2z \\ a_{33} &= 11.0889 + x + z \\ a_{44} &= 3.1329 + 0.5x + 0.5z \\ a_{13} &= 1.8148 + 0.5x + 0.5z \end{aligned}$$

See Figure 5 to Figure 8.

In Table (1),the relative maximum errors and their convergence rates with respect to h are presented. Because the analytic solution is not known, the TT solution with the finest grid ($h = 0.00125$) is used as the analytic solution. Then the relative errors in the computed TT are defined as

$$E(\tau, h) = \frac{\|\tau_{analytic} - \tau^h_{FD}\|_\infty}{\|\tau_{analytic}\|_\infty}$$

where $\tau_{analytic}$ and τ_{FD} are analytic and finite difference solutions. The convergence

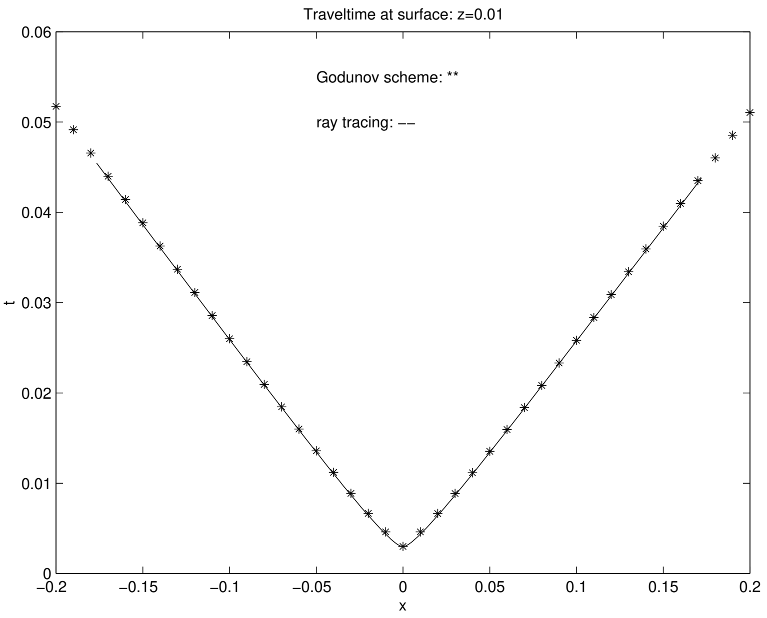

FIG. 6. ENO TT and Raytracing TT near surface:Example 2

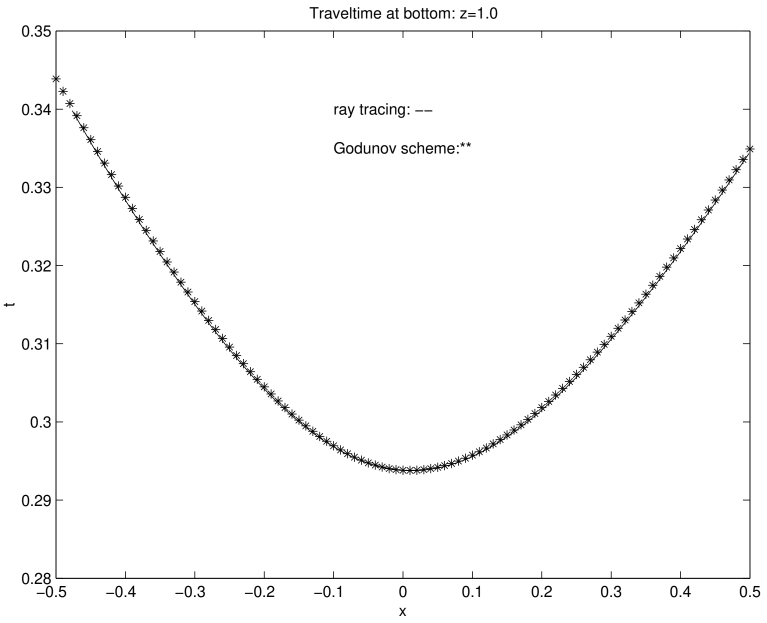

FIG. 7. ENO TT and Raytracing TT at bottom:Example 2

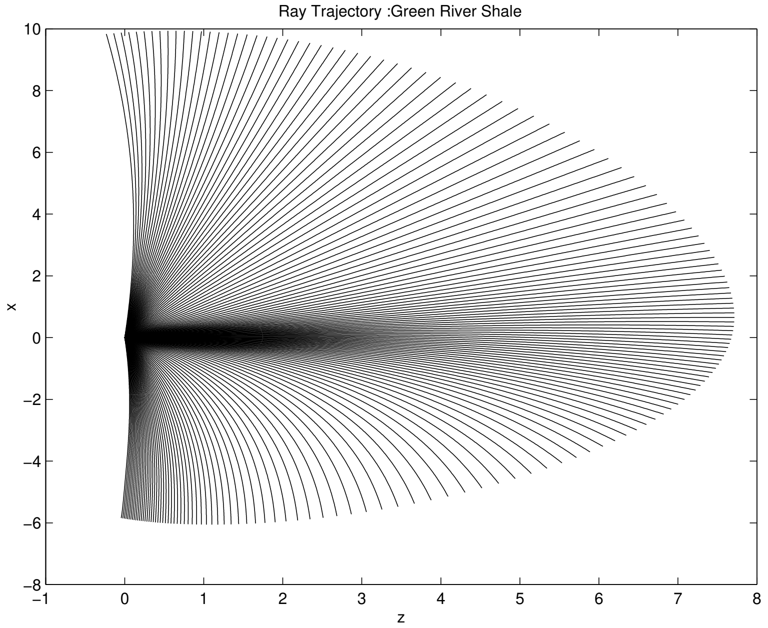

FIG. 8. Raytracing:Example 2

rates α are given as

$$\alpha(\tau, h) \quad = \quad \frac{\log\left(\frac{E(\tau,2h)}{E(\tau,h)}\right)}{\log 2}.$$

Because we used an approximation to exact solution to measure the convergence rate, the exact second order convergence rate could not be observed, however, the convergence rate asymtotically increases towards 2.

Example 3. The four elastic parameters are:

$$\begin{aligned} a_{11} &= 15.3871 + 2z \\ a_{33} &= 14.5161 + z \\ a_{44} &= 5.6074 + 0.5z \\ a_{13} &= 3.9321 + 0.5z \end{aligned}$$

The corresponding Thomsen's parameters for homogeneous Bandera Sandstone are

$$\begin{aligned} \alpha_0 &= 3.8km/s, \\ \beta_0 &= 2.4km/s, \\ \epsilon &= 0.030, \\ \delta &= 0.045. \end{aligned}$$

See Figure 9 to Figure 12.

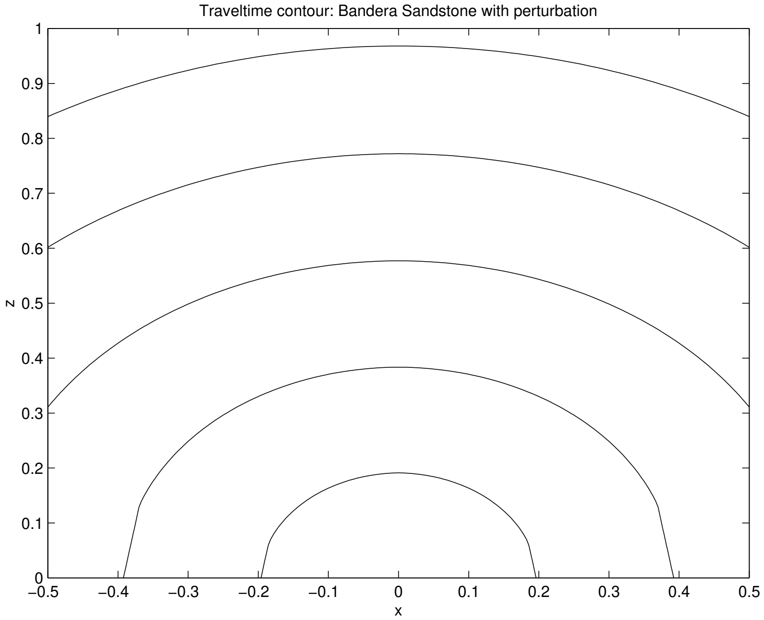

FIG. 9. Wavefront: Example 3

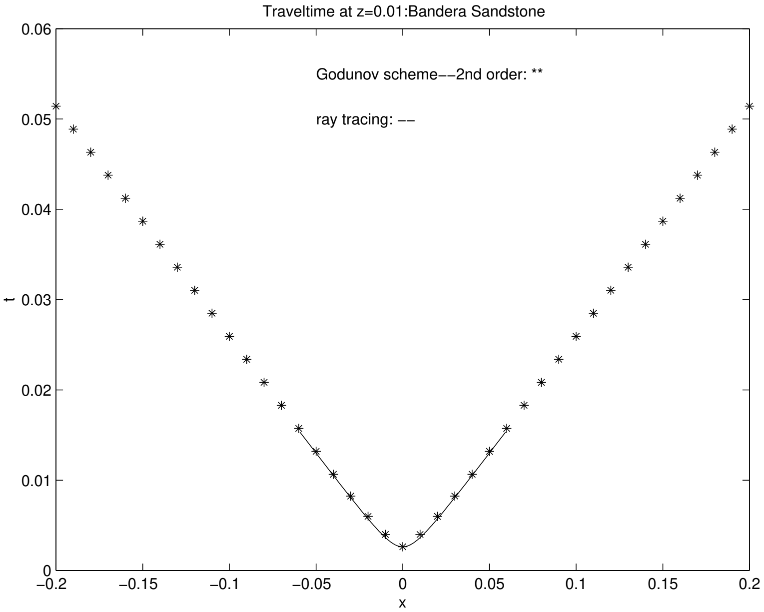

FIG. 10. ENO TT and Raytracing TT near surface:Example 3

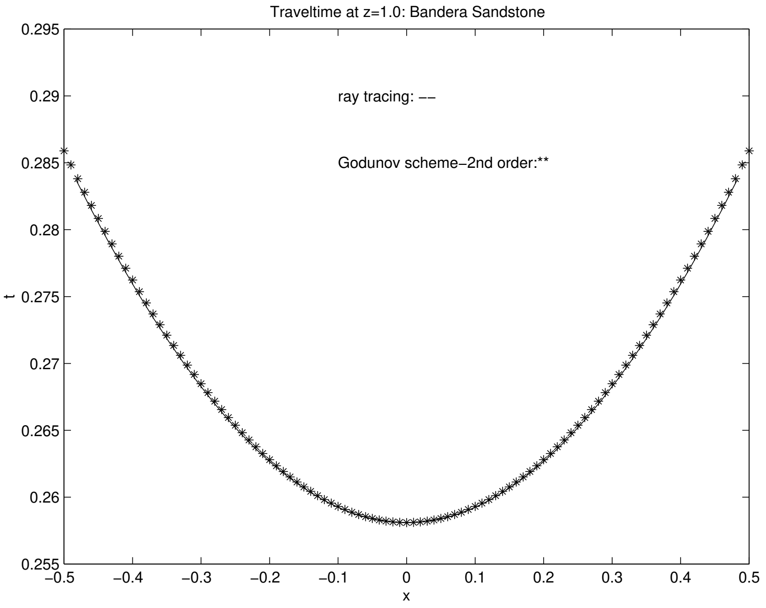

FIG. 11. ENO TT and Raytracing TT at bottom:Example 3

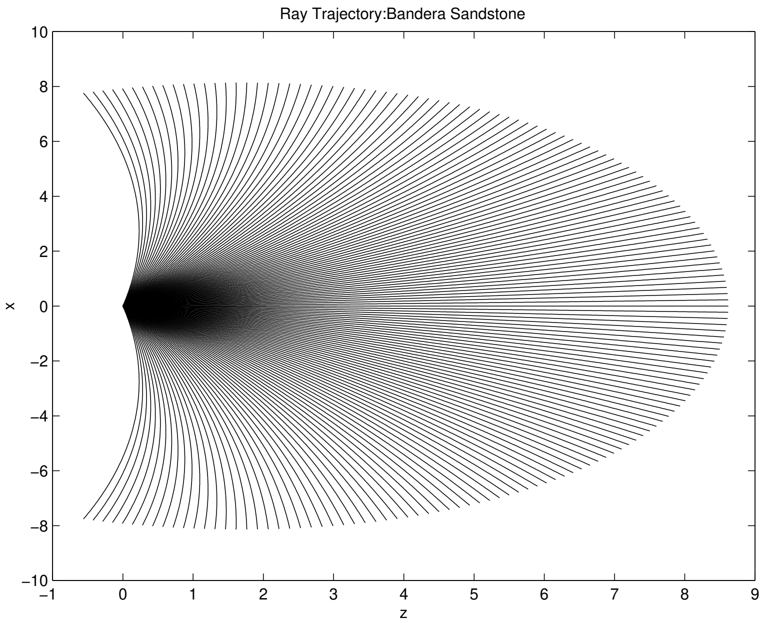

FIG. 12. Raytracing:Example 3

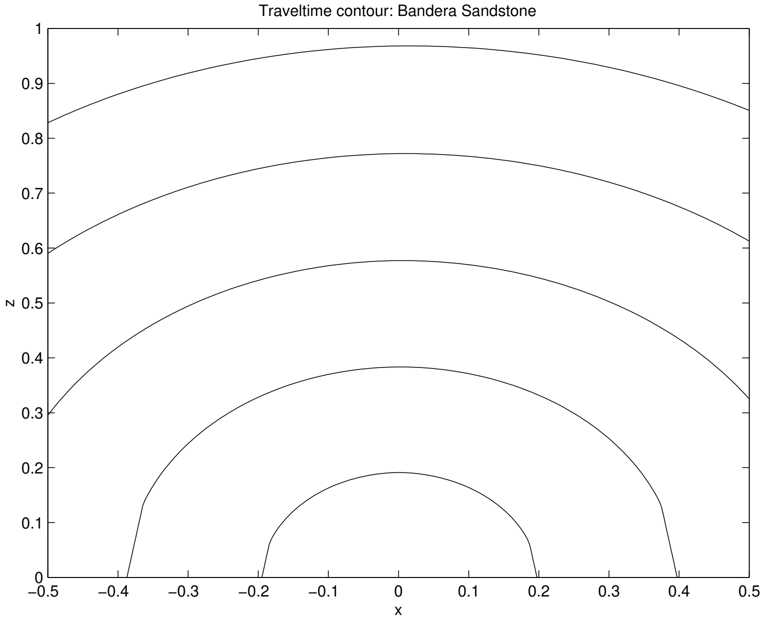

FIG. 13. Wavefront: Example 4

Example 4. The four elastic parameters are :

$$\begin{aligned} a_{11} &= 15.3871 + 2x + 2z \\ a_{33} &= 14.5161 + x + z \\ a_{44} &= 5.6074 + 0.5x + 0.5z \\ a_{13} &= 3.9321 + 0.5x + 0.5z \end{aligned}$$

See Figure 13 to Figure 16.

Numerical Experiments: 3D VTI media

Several three dimensional experiments are presented to show that our approach is feasible and promising.

In all examples,traveltimes for qP wave propagation in VTI media are computed. All models occupy the cube $\{-0.5km \leq x \leq 0.5km, -0.5km \leq y \leq 0.5km, 0 \leq z \leq 1.5km\}$,the source is located at the center of the surface ($z = 0$).The maximum phase angle is taken as $\theta_{\max} = 6.5\pi/18$. The ray-tracing system using depth as running parameter is used to calibrate our codes (See Appendix A).

Example 5. Homogeneous Green River Shale with Thomsen's parameters:

$$\alpha_0 = 3.33km/s,$$

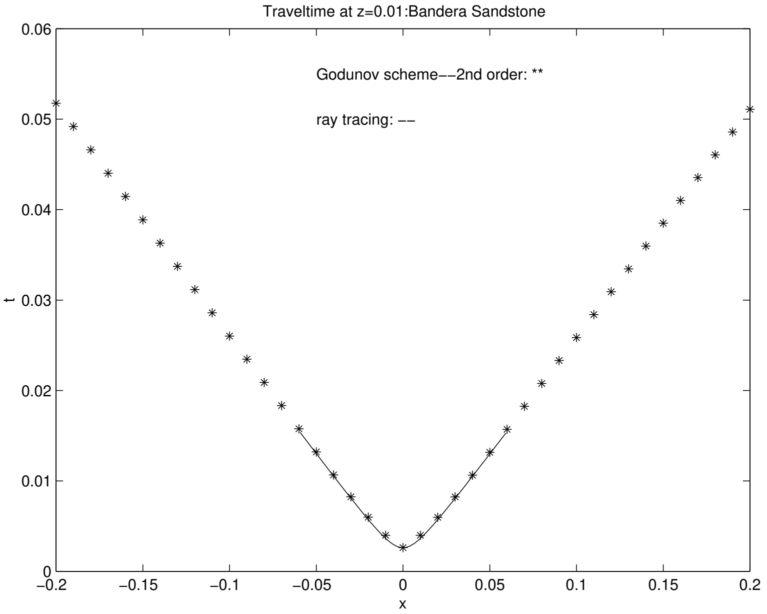

FIG. 14. ENO TT and Raytracing TT near surface: Example 4

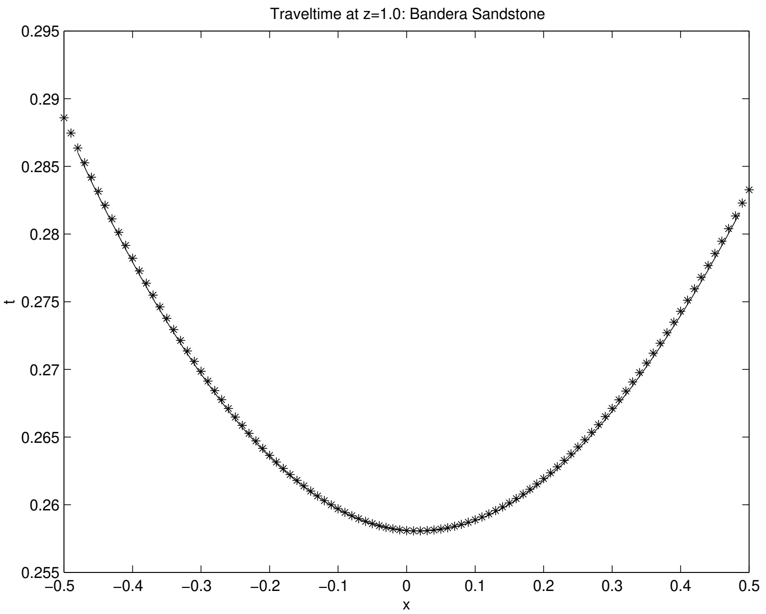

FIG. 15. ENO TT and Raytracing TT at bottom:Example 4

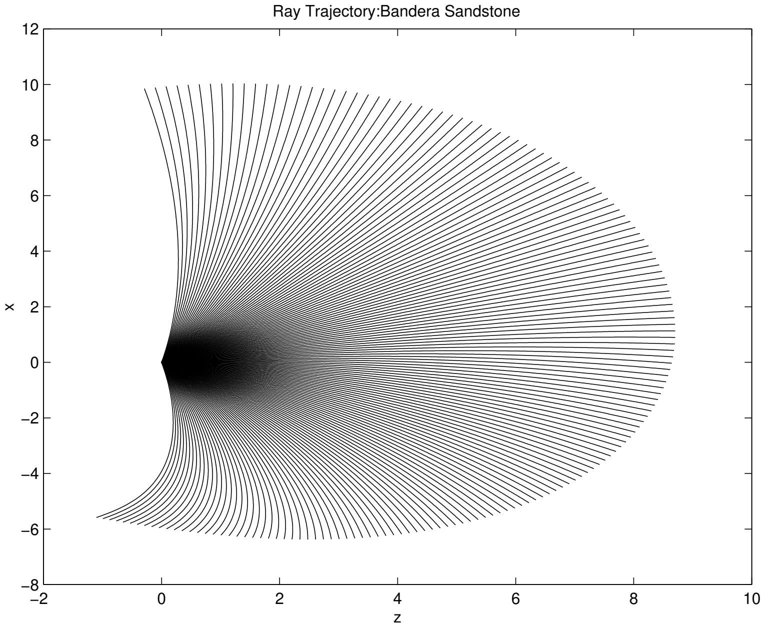

FIG. 16. Raytracing: Example 4

$$\begin{aligned}\beta_0 &= 1.77km/s,\\ \epsilon &= 0.195,\\ \delta &= -0.220.\end{aligned}$$

$\Delta x = \Delta y = \Delta z = 0.0125.$

See Figure 17 to Figure 20.

Example 6. Homogeneous Mesa sandstone with Thomsen's parameters:

$$\begin{aligned}\alpha_0 &= 3.79km/s,\\ \beta_0 &= 2.07km/s,\\ \epsilon &= 0.189,\\ \delta &= 0.204.\end{aligned}$$

$\Delta x = \Delta y = \Delta z = 0.0125.$

See Figure 21 to Figure 24.

Example 7. The four elastic parameters are:

$$\begin{aligned}a_{11} &= 15.4136 + 2z\\ a_{33} &= 11.0889 + z\\ a_{44} &= 3.1329 + 0.5z\\ a_{13} &= 1.8148 + 0.5z\end{aligned}$$

$\Delta x = \Delta y = \Delta z = 0.05.$

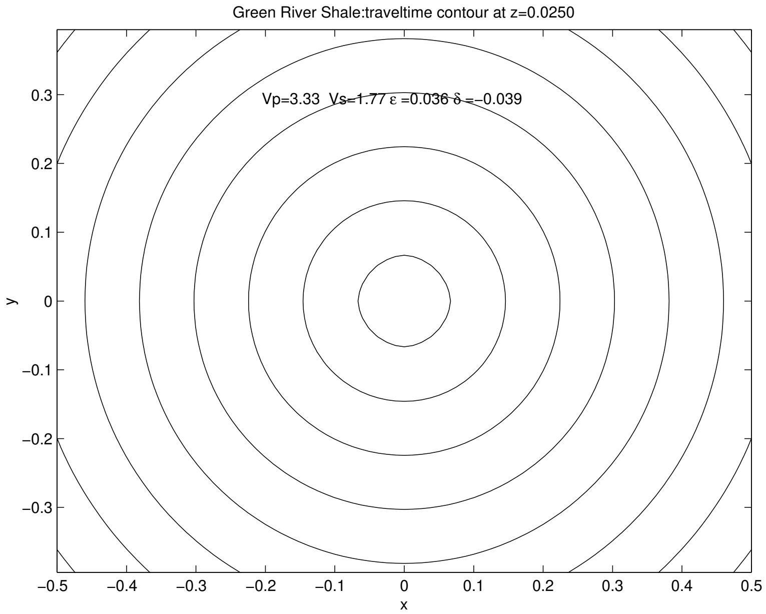

FIG. 17. Wavefront near surface:Green River Shale

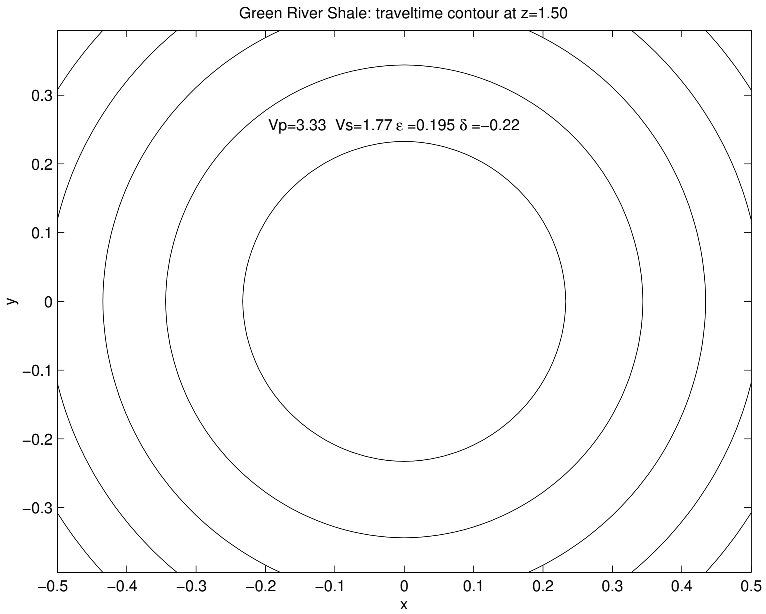

FIG. 18. Wavefront at bottom: Green River Shale

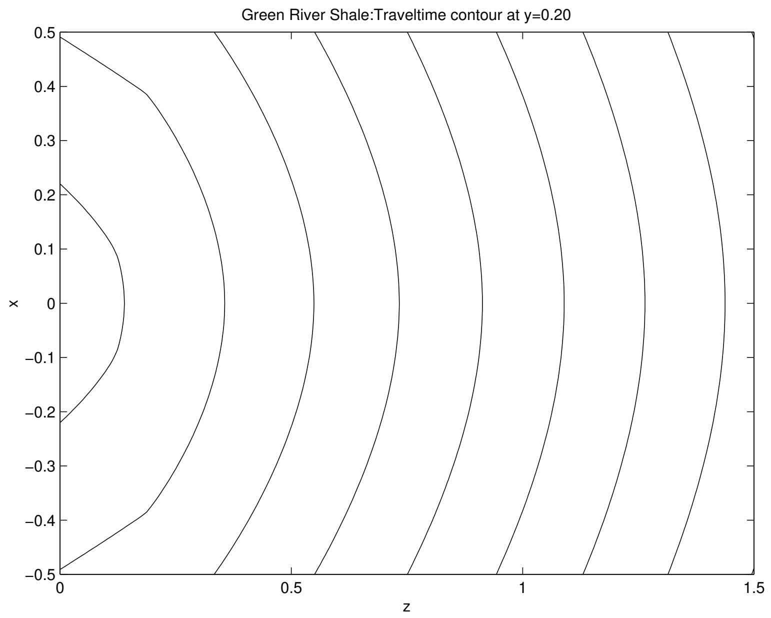

FIG. 19. Wavefront profile: Green River Shale

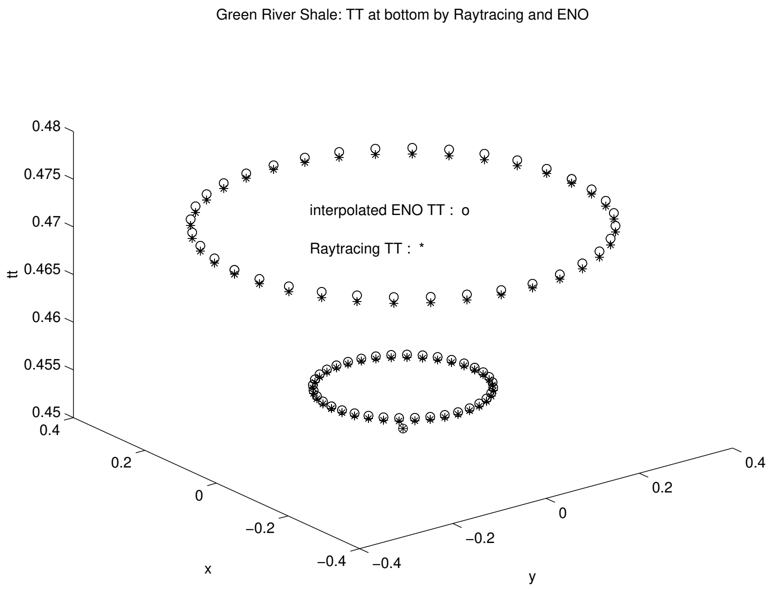

FIG. 20. ENO TT and Raytracing TT: Green River shale

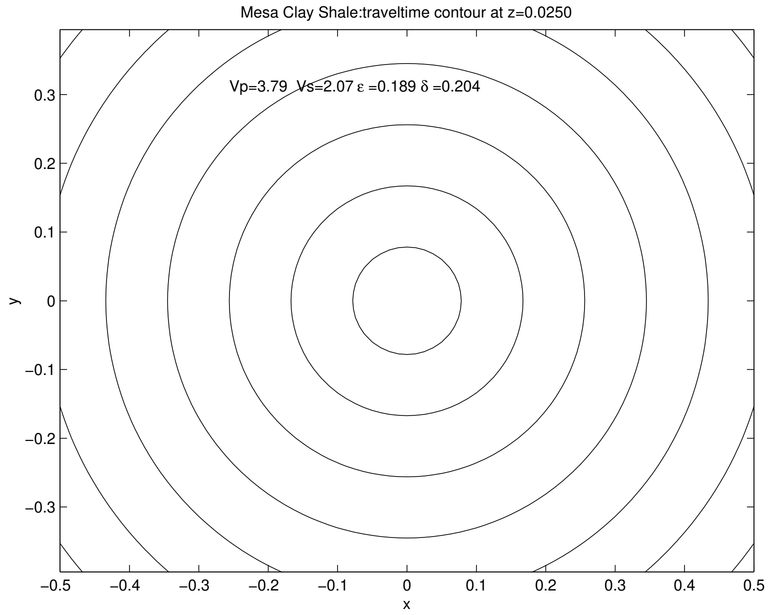

FIG. 21. Wavefront near surface:Mesa Sandstone

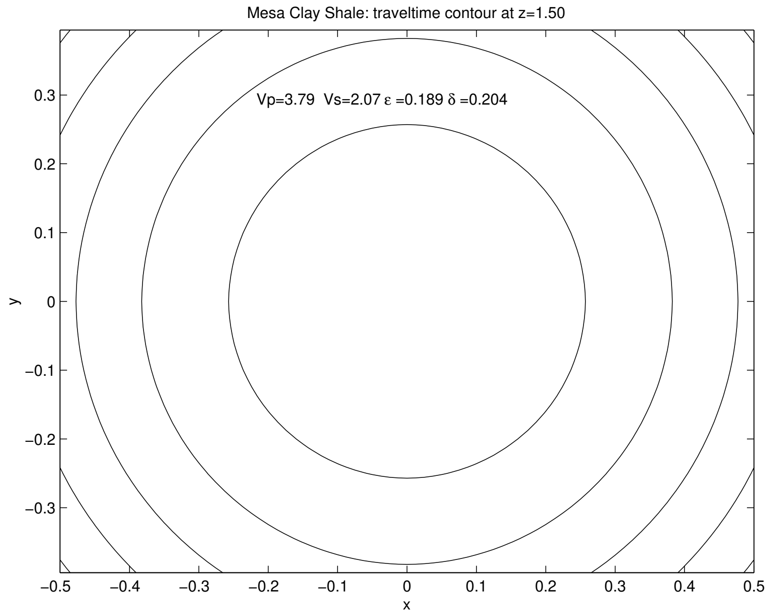

FIG. 22. Wavefront at bottom: Mesa Sandstone

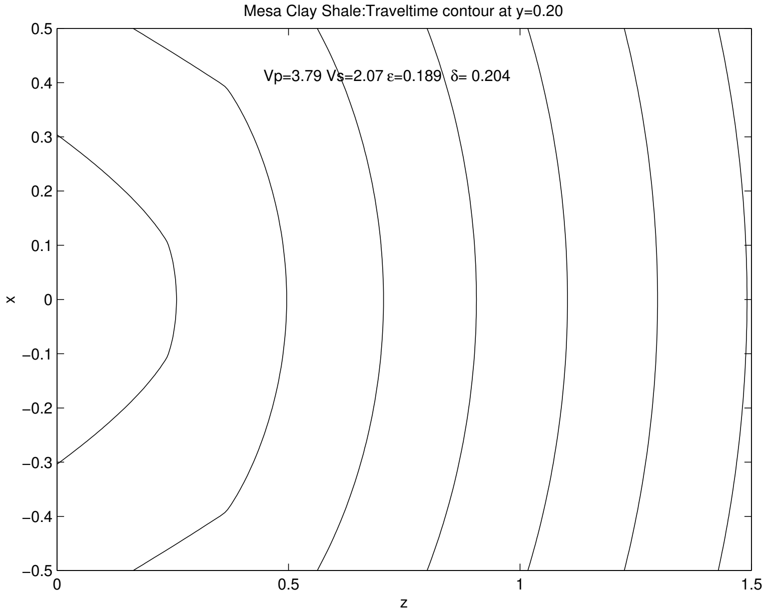

FIG. 23. Wavefront profile: Mesa Sandstone

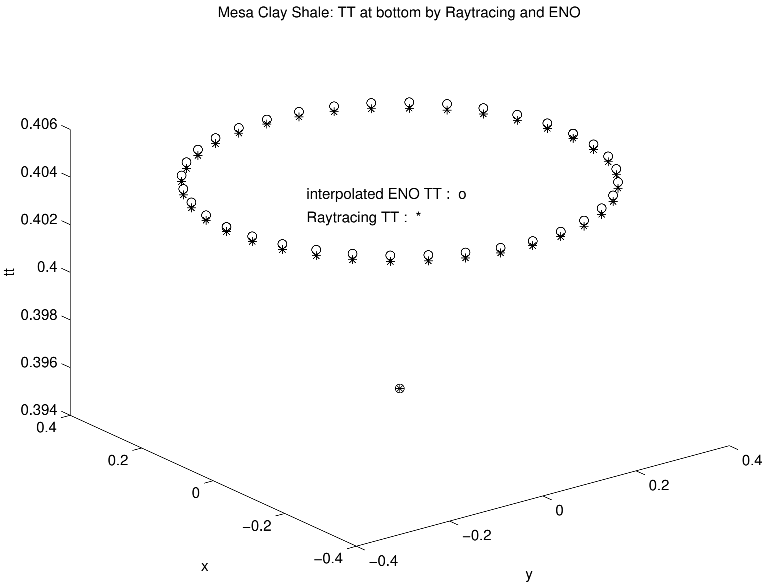

FIG. 24. ENO TT and Raytracing TT: Mesa sandstone

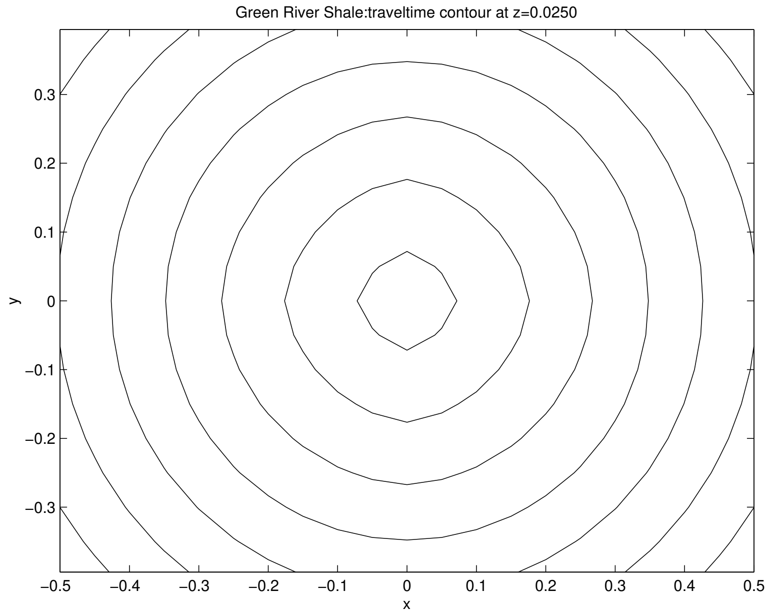

Fig. 25. Wavefront near surface:Example 7

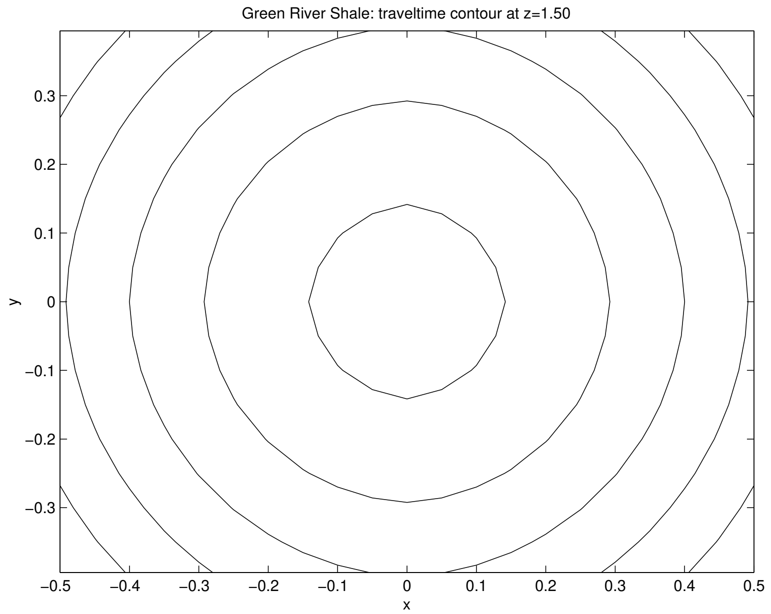

Fig. 26. Wavefront at bottom:Example 7

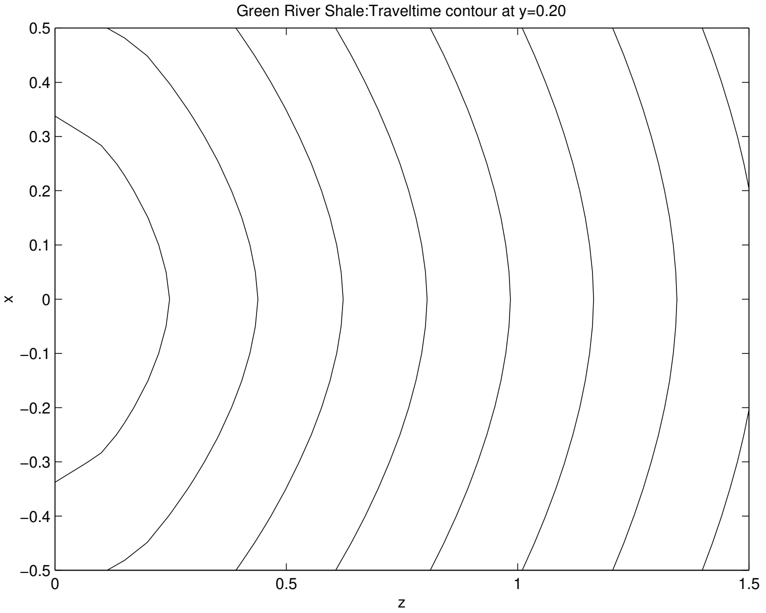

FIG. 27. Wavefront profile:Example 7

See Figure 25 to Figure 27.

Example 8. The four elastic parameters are the same as Example 7,but meshsizes are $\Delta x = \Delta y = \Delta z = 0.0125$.

See Figure 28 to Figure 30.

Isotropic and Anisotropic Marmousi Model

We tested our method on the original isotropic and the anisotropic Marmousi model created by (Alkhalifah, 1997) [1].

The Marmousi model occupies the rectangle $\{0km \leq x \leq 9.2km, 0 \leq z \leq 2.9875km\}$,the lateral and depth samples are 737 and 240 respectively so that the sampling interval both laterally and vertically are equal to 12.5 meters. The original isotropic Marmousi velocity model is presented in Figure 31 and the anisotropic Marmousi η model is shown in Figure 32.

In the computation,maximum aperture angle is taken as $\theta_{\max} = 3.75\pi/9$.

Example 9. Isotropic and Anisotropic Marmousi Model.

Source is located at $(x = 3.0km, z = 0.0km)$.See Figure 33 to Figure 34.

Example 10. Isotropic and Anisotropic Marmousi Model.

Source is located at $(x = 6.0km, z = 0.0km)$.

[1] $http://sepwww.stanford.edu/sep/tariq/Html\_marmousi/marmousi\_ti.html$

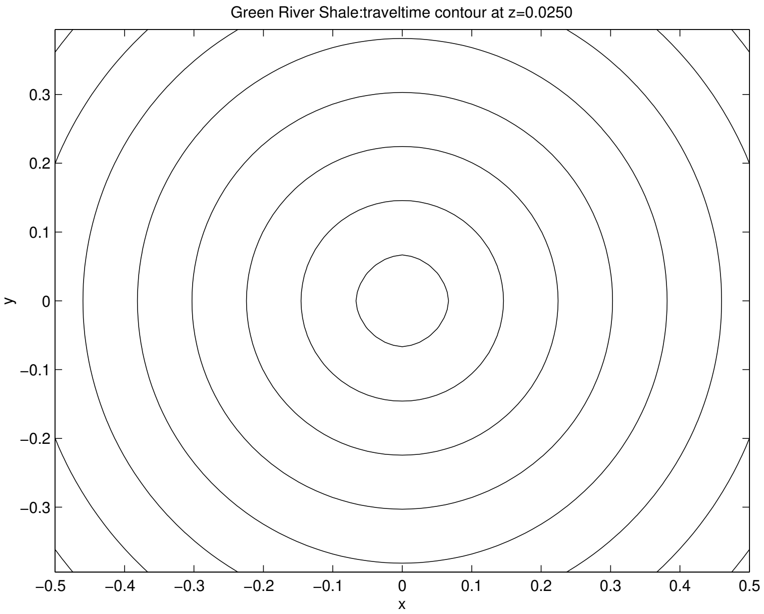

Fig. 28. Wavefront near surface:Example 8

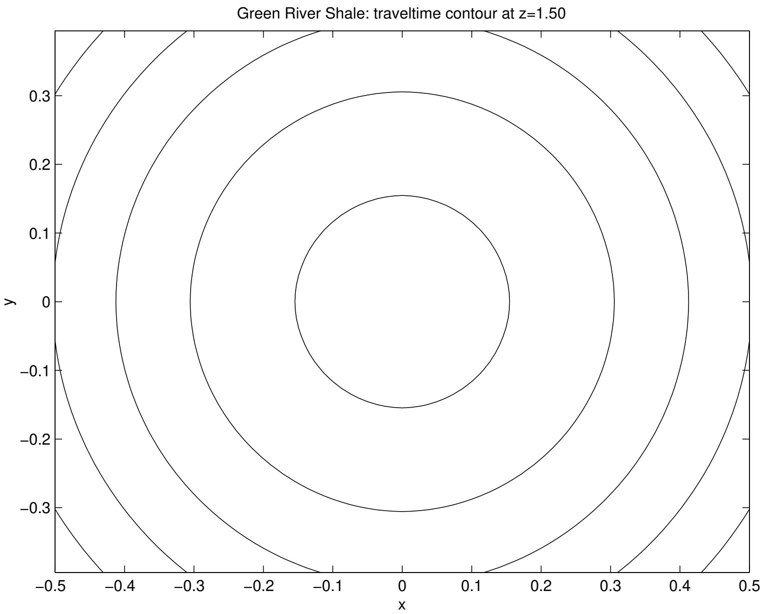

Fig. 29. Wavefront at bottom:Example 8

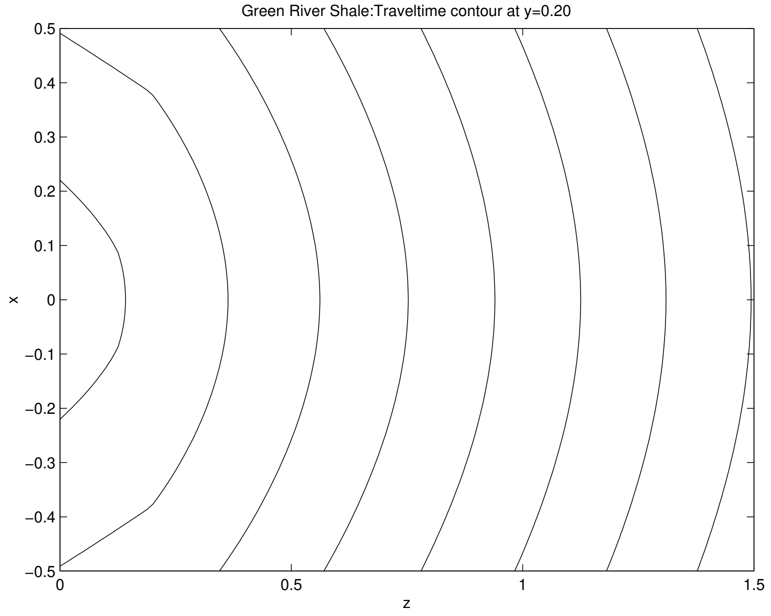

FIG. 30. Wavefront profile:Example 8

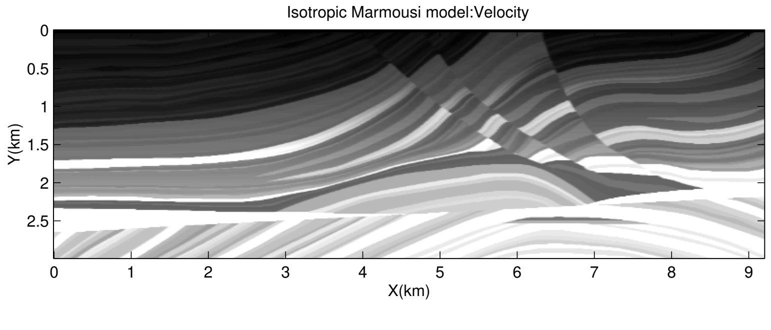

FIG. 31. Isotropic Marmousi model: Velocity

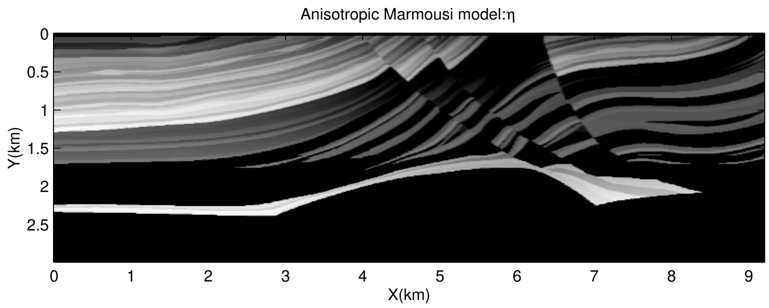

FIG. 32. Anisotropic Marmousi model: η

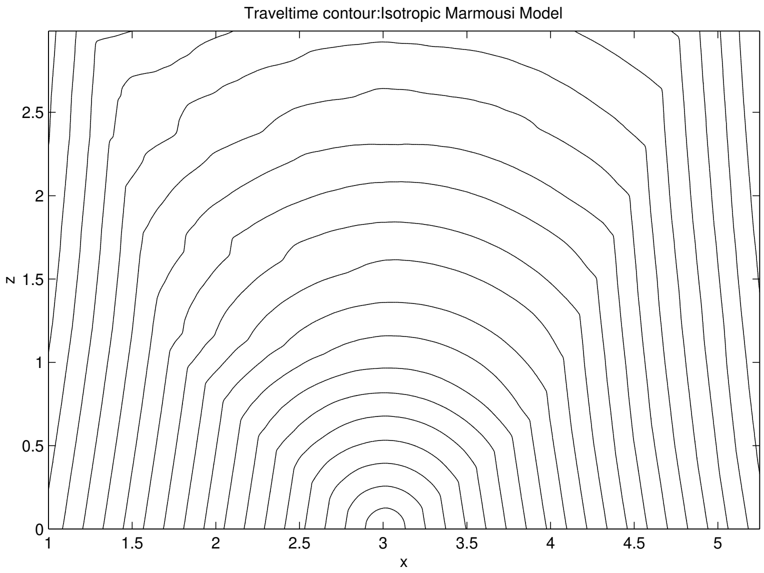

FIG. 33. Wavefront:Isotropic Marmousi model

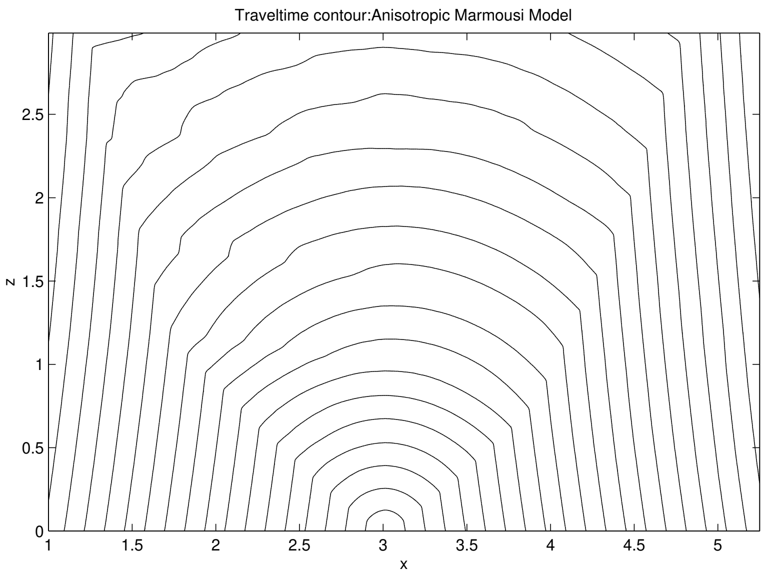

Fig. 34. Wavefront:Anisotropic Marmousi model

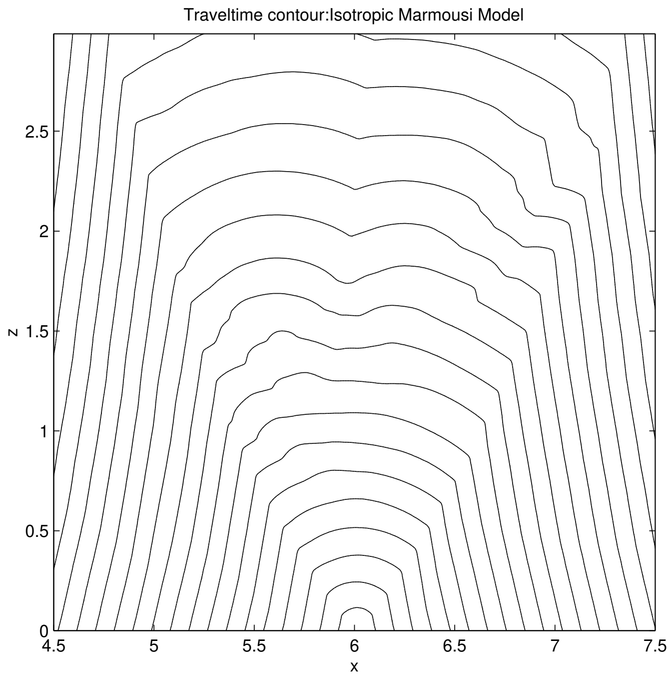

Fig. 35. Wavefront:Isotropic Marmousi model

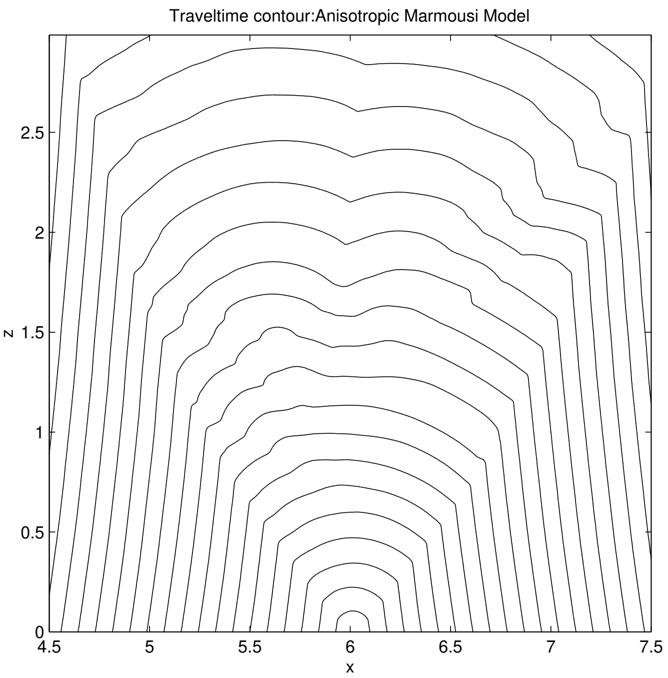

FIG. 36. Wavefront:Anisotropic Marmousi model

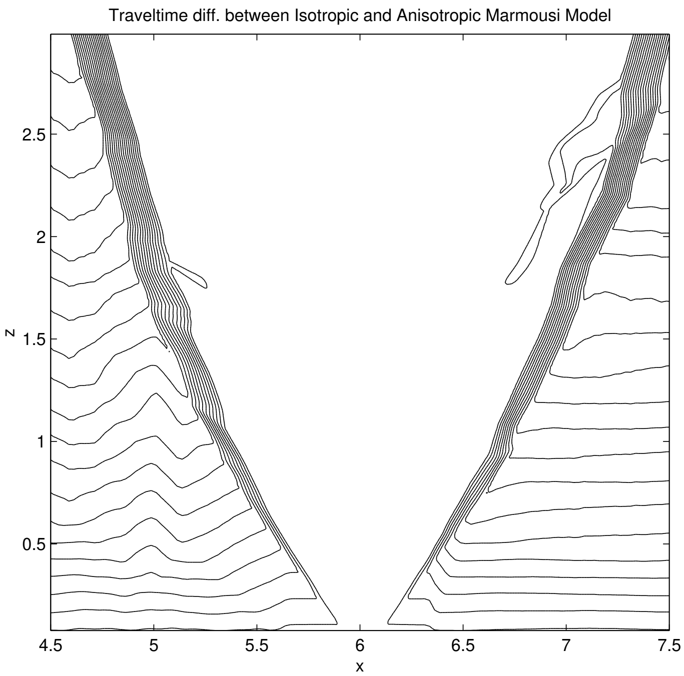

FIG. 37. Difference of Traveltime between Isotropic and Anisotropic Marmousi model

See Figure 35 and Figure 36. Because the vertical velocity is the same for the anisotropic and isotropic Marmousi models, the portion of the wavefront corresponding to vertical wave propagation is similar,which we can see by subtracting the two traveltime fields,with results shown in Figure 37.

Conclusion

We have just used a second order upwind finite difference scheme for the computation of traveltime in 2D and 3D VTI media. Also we tested our method on the isotropic and an anisotropic Marmousi model. Both numerical experiments and tests on synthetic model showed our approach is efficient and accurate.

We will use similar schemes to compute the amplitude in 3D VTI media very soon.

When we have the traveltime and amplitude in 3D VTI media at our disposal,we want to use them in the high frequency asymptotic imaging techniques such as Kirchhoff migration method for imaging/inversion in reflection seismology (Beylkin, 1985; Symes et al., 1994; Symes, 1995).

Also with the traveltime and amplitude at hand,we want to generalize DSO (differential semblance optimization)(Symes and Carazzone, 1991; Symes, 1990) for the velocity analysis in the isotropic media to the anisotropic media.

Because all our design is based upon the assumption that the first-arrival traveltime corresponding to qP wave propagation in anisotropic media is the viscosity solution of some Hamilton-Jacobi equation (Lions, 1982; Evans, 1994),we need to prove it theoretically in the case of VTI media.

Many subsurface media are transversely isotropic but with arbitrary symmetric axis, it is necessary to consider the computation of traveltime and amplitude in 3D TI media with arbitrary symmetric axis.

More interesting case is how to implement our formulations (Qian and Symes, 1998) efficiently in general 3D anisotropic media.

Acknowledgement and Disclaimer: This work was partially supported by the National Science Foundation under grant number DMS 9627355; the Office of Naval Research under grant number N00014-96-1-0156; the Air Force Office of Scientific Research, Air Force Materials Command, USAF, under grant number F49620-95-1-0339; and The Rice Inversion Project. TRIP Sponsors for 1998 are Amerada Hess, ARCO E & P Technology, Amoco Production Co., Conoco Inc., Exxon Production Research Co., Interactive Network Technologies, Landmark Graphics, Mobil Technology Co., and Shell International Research. The US Government is authorized to reproduce and distribute reprints for governmental purposes notwithstanding any copyright notation thereon. The views and conclusions contained herein are those of the authors and should not be interpreted as necessarily representing the official policies or endorsements, either expressed or implied, of the Air Force Office of Scientific Research, the Office of Naval Research, the National Science Foundation, or the US Government.

REFERENCES

Alkhalifah, T. (1996). *Seismic Processing in Transversely Isotropic Media.* PhD thesis, Center for Wave Phenomena,Colorado School of Mines, Golden,Co80401-1887.

Alkhalifah, T. (1997). An acoustic wave equation for anisotropic media. Sep95,pp 283-308, Stanford Exploration Project.

Anderson, J. (1996). *Imaging in Transversely Isotropic Media with a Vertical Symmetry Axis.* PhD thesis, Center for Wave Phenomena,Colorado School of Mines, Golden,Co80401-1887.

Berryman, J. G. (1979). Long-wave elastic anisotropy in transversely isotropic media. *Geophysics*, 44:896–917.

Beylkin, G. (1985). Imaging of discontinuities in the inverse scattering problem by inversion of a causal generalized radon transform. *J. Math. Phys.*, 26:99–108.

Cerveny, V. (1972). Seismic rays and ray intensities in inhomogeneous anisotropic media. *Geophys. J. R.Astr.Soc.*, 29:1–13.

Cerveny, V. and Psencik, I. (1972). Rays and travel-time curves in inhomogeneous anisotropic media. *Zeitschrift fur Geophysik*, 38:565–577.

Crandall, M., L.C.Evans, and Lions, P. (1984). Some properties of viscosity solutions of hamilton-jacobi equations. *Trans. Amer. Math. Soc.*, 282:487–502.

Crandall, M. and Lions, P. (1983). Viscosity solutions of hamilton-jacobi equations. *Trans. Amer. Math. Soc.*, 277:1–42.

Dellinger, J. (1991). Anisotropic finite-difference traveltimes. In *61th Annual Internat.Mtg. Expanded Abstracts*, pages 1530–1533. Soc.Expl.Geophys.

Dellinger, J. and Symes, W. (1997). Anisotropic finite-difference traveltimes using a hamilton-jacobi solver. In *67th Annual Internat.Mtg. Expanded Abstracts*, pages 1786–1789. Soc.Expl.Geophys.

El-Mageed, M. (1996). *3 D First arrival traveltimes and amplitudes via Eikonal and Transport Finite differences solvers.* PhD thesis, Department of Computational and Applied mathematics,Rice University, Houston,TX77251-1892.

El-Mageed, M., Kim, S., and Symes, W. (1997). 3-d kirchhoff migration using finite difference traveltimes and amplitudes. Trip annual report, The Rice Inversion Project,Rice University, Houston,TX77005.

Evans, L. (1994). *Partial differential equations*. Berkley Mathematics Lecture Notes.

Kim, S. and Cook, R. (1998). Second-order finite difference traveltimes in three dimensions. Technical report, Shell E&P Technology Co., Houston,TX77001-0481.

LeVeque, R. (1990). *Numerical methods for conservation laws*. Birkhauser-Verlag.

Lions, P. (1982). *Generalized solutions of Hamilton-Jacobi equations*. Pitman Advanced Publishing Program.

Musgrave, M. (1970). *Crystal Acoustics*. Holden-Day.

Osher, S. and Sethian, J. (1988). Fronts propagating with curvature dependent speed:algorithms based on hamilton-jacobi formulations. *J. Comput. Phys.*, 79:12–49.

Osher, S. and Shu, C. (1991). High-order essentially nonoscillatory schemes for hamilton-jacobi equations. *SIAM J. Num. Anal.*, 28:907–922.

Qian, J. and Symes, W. (1998). Hamilton-jacobi equations and upwind finite difference schemes for traveltime and amplitude in inhomogeneous anisotropic media: Mathematical formulations. Technical report, The Rice Inversion Project,Rice University,Houston,TX77005.

Reshef, M. and Kosloff, D. (1986). Migration of common shot gathers. *Geophysics*, 51:324–331.

Schneider, W. (1995). Robust and efficient upwind finite-difference traveltime calculations in three dimensions. *Geophysics*, 60:1108–1117.

Shu, C. and Osher, S. (1988). Efficient implementation of essentially non-oscillatory shock capturing schemes. *J. Comput. Phys.*, 77:439–471.

Strikwerda, J. (1989). *Finite Difference Schemes and Partial Differential Equations*. Wadsworth-Brooks/Cole,Pacific Grove,California.

Symes, W. (1990). Velocity inversion: A case study in infinite-dimensional optimization. *Math. Programming.*, 48:71–102.

Symes, W. (1995). Mathematics of reflection seismology. Trip technical report, The Rice Inversion Project,Rice University, Houston,TX77005.

Symes, W. and Carazzone, J. (1991). Velocity inversion by differential semblance optimization. *Geophysics*, 56:654–663.

Symes, W., Versteeg, R., Sei, A., and Tran, Q.-H. (1994). Kirchhoff simulation,migration and inversion using finite difference traveltimes and amplitudes. Trip annual report, The Rice Inversion Project,Rice University, Houston,TX77005.

Thomsen, L. (1986). Weak elastic anisotropy. *Geophysics*, 51:1954–1966.

Tsvankin, I.and Thomsen, L. (1995). Inversion of reflection traveltimes for transverse isotropy. *Geophysics*, 60:1095–1107.

van Trier, J. and Symes, W. (1991). Upwind finite-difference calculation of traveltimes. *Geophysics*, 56:812–821.

Vidale, J. (1988). Finite-difference calculation of travel times. *Bull.,Seis. Soc. Am.*, 78:2062–2076.

Appendix A. RAY TRACING SYSTEM IN 3D VTI

To calibrate our finite difference code for eikonal equation,we need a ray tracing system using depth as a running parameter along the ray. By eikonal equation (1) for 3D VTI and $p_3 > 0$, define Hamiltonian

$$G(x_1, x_2, x_3, p_1, p_2, p_3) = p_3 - H(p_1, p_2) \tag{A-1}$$

then by the method of characteristics we have

$$\frac{dx_1}{dx_3} = \frac{r_1}{r_3} \tag{A-2}$$

$$\frac{dx_2}{dx_3} = \frac{r_2}{r_3} \tag{A-3}$$

$$\frac{d\tau}{dx_3} = p_3 + \frac{r_1}{r_3}p_1 + \frac{r_2}{r_3}p_2 \tag{A-4}$$

$$\frac{dp_1}{dx_3} = \frac{t_1}{2r_3} \tag{A-5}$$

$$\frac{dp_2}{dx_3} = \frac{t_2}{2r_3} \tag{A-6}$$

$$\frac{dp_3}{dx_3} = \frac{t_3}{2r_3} \tag{A-7}$$

where

$$
\begin{aligned}
r_1 &= p_1(2a_{11}a_{44}(p_1^2+p_2^2)+Ap_3^2-a_{11}-a_{44}) \\
r_2 &= p_2(2a_{11}a_{44}(p_1^2+p_2^2)+Ap_3^2-a_{11}-a_{44}), \\
r_3 &= p_3(2a_{33}a_{44}p_3^2+A(p_1^2+p_2^2)-a_{33}-a_{44}), \\
t_1 &= \frac{\partial a_{11}}{\partial x_1}(p_1^2+p_2^2)D_2+\frac{\partial a_{33}}{\partial x_1}p_3^2D_1+\frac{\partial a_{44}}{\partial x_1}F+2\frac{\partial a_{13}}{\partial x_1}(p_1^2+p_2^2)p_3^2(a_{13}+a_{44}), \\
t_2 &= \frac{\partial a_{11}}{\partial x_2}(p_1^2+p_2^2)D_2+\frac{\partial a_{33}}{\partial x_2}p_3^2D_1+\frac{\partial a_{44}}{\partial x_2}F+2\frac{\partial a_{13}}{\partial x_2}(p_1^2+p_2^2)p_3^2(a_{13}+a_{44}), \\
t_3 &= \frac{\partial a_{11}}{\partial x_3}(p_1^2+p_2^2)D_2+\frac{\partial a_{33}}{\partial x_3}p_3^2D_1+\frac{\partial a_{44}}{\partial x_3}F+2\frac{\partial a_{13}}{\partial x_3}(p_1^2+p_2^2)p_3^2(a_{13}+a_{44}), \\
A &= a_{11}a_{33}+a_{44}^2-(a_{13}+a_{44})^2, \\
D_1 &= 1-a_{11}(p_1^2+p_2^2)-a_{44}p_3^2, \\
D_2 &= 1-a_{44}(p_1^2+p_2^2)-a_{33}p_3^2, \\
F &= p_1^2+p_2^2+p_3^2-a_{11}(p_1^2+p_2^2)^2-a_{33}p_3^4+2a_{13}(p_1^2+p_2^2)p_3^2.
\end{aligned}
\tag{A-8}
$$